Waste Management 120 (2021) 303–313

Contents lists available at ScienceDirect

Waste Management

journal homepage: www.elsevier.com/locate/wasman

Characterization of hydrochar and process water from the hydrothermal carbonization of Refuse Derived Fuel

Catarina Nobre [a,*], Octávio Alves [a,b], Luís Durão [a,b], Ali Şen [c], Cândida Vilarinho [d], Margarida Gonçalves [a,b]

[a] MEtRICs, Mechanical Engineering and Resource Sustainability Center, Department of Science and Technology of Biomass, FCT- NOVA University of Lisbon, 2829-516 Caparica, Portugal
[b] VALORIZA, Research Centre for Endogenous Resource Valorization, Polytechnic Institute of Portalegre, 7300-555 Portalegre, Portugal
[c] Forest Research Centre, School of Agriculture, University of Lisbon, Tapada da Ajuda, 1349-017 Lisboa, Portugal
[d] MEtRICs, Mechanical Engineering and Resource Sustainability Center, Mechanical Engineering Department, School of Engineering, University of Minho, 4804-533 Guimarães, Portugal

ARTICLE INFO

Article history:
Received 29 July 2020
Revised 27 October 2020
Accepted 13 November 2020
Available online 14 December 2020

Keywords:
Refuse Derived Fuel
Hydrothermal carbonization
Alternative solid fuel
Hydrochar
Process water

ABSTRACT

In this study, hydrothermal carbonization (HTC) was used as a thermochemical conversion process to upgrade Refuse Derived Fuel (RDF). The effect of process temperature (250 °C, 275 °C and 300 °C), residence time (30 min and 120 min), and RDF-to-water ratio (1:15 and 1:5) on the main characteristics of the produced hydrochars and process waters was assessed. The HTC process yielded hydrochars with enhanced fuel properties when compared to the original feedstock, namely higher carbon content and heating value. The hydrochars also presented reduced oxygen and ash contents. The hydrochar produced at 300 °C for 120 min presented the lowest ash content (3.3 wt%, db) whereas the highest heating value was found for the hydrochar obtained at 275 °C for 120 min (28.1 MJ/kg, db). The HTC process was also responsible for a significant reduction in chlorine concentration, showing dechlorination efficiencies between 69.2 and 77.9%. However, the HTC process generated acidic process waters with high COD values (maximum 27.2 gO_2/L), which need to be further managed or valorized. Energy calculations were also performed, revealing that lower water amounts, lower temperatures, and longer residence times, represent optimal conditions for higher hydrochar yields and consequently good process efficiencies.

1. Introduction

Effective energy recovery from wastes could be reached by the production of waste derived fuels such as Refuse Derived Fuel (RDF). RDF is the fuel product obtained from the treatment of non-hazardous wastes streams, such as municipal solid wastes (MSW) or regular industrial wastes (Násner et al., 2017). RDF frequently contains a variety of plastics and other miscellaneous components that can strongly increase its chlorine and ash contents (Ma et al., 2010; Nobre et al., 2019a; Reza et al., 2013). These characteristics are restrictive regarding thermochemical conversion processes for energy production, which is the main goal of RDF production. During combustion or gasification processes, the presence of chlorine in excess may produce gaseous HCl that corrodes and forms deposits in downstream equipment, whereas ash with high fusibilities at high temperatures promotes slagging problems and reduces the performance of such processes (Silva et al., 2014; You et al., 2017). Polymeric materials contained in RDF may accentuate the formation of undesirable tars after gasification (Kobayashi et al., 2011; Zaccariello and Mastellone, 2015). Therefore, it is imperative to define alternative solutions that can attenuate these issues in waste-to-energy technologies.

Traditional thermochemical conversion techniques such as torrefaction or carbonization may reduce chlorine content, but they increase ash content due to the elimination of volatiles (Yuan et al., 2015). On the other hand, hydrothermal carbonization (HTC) allows for a material densification of lignocellulosic and polymeric materials while reducing their ash content by partial dissolution in the process water (Wang et al., 2020). Thus, HTC enables an upgrading effect that is not possible with the previously mentioned thermochemical processes (Lin et al., 2017).

The HTC process takes place at relatively low temperatures (180–350 °C), variable residence times (from 30 min to several hours) and under autogenous pressure (Wang et al., 2018a). During this process, the feedstock undergoes different reactions, such as hydrolysis, dehydration, decarboxylation, aromatization and re-

* Corresponding author: Department of Science and Technology of Biomass, FCT-NOVA University of Lisbon, 2829-516 Caparica, Portugal.
E-mail address: cp.nobre@campus.fct.unl.pt (C. Nobre).

https://doi.org/10.1016/j.wasman.2020.11.040
0956-053X/

condensation (Li et al., 2013; Mohammed et al., 2020). These reactions are responsible for significant increases in carbon content and decreases in oxygen content of the feedstock (Krysanova et al., 2019). HTC generates solid (hydrochar), liquid (process water) and gaseous (mainly CO_2) products (Wilk et al., 2020). Hydrochar is generally considered a good feedstock for energy production due to its high carbon content, heating value and hydrophobicity. Besides, the lower amounts of oxygen reduce the formation of harmful nitrogen and sulphur oxides after posterior energy conversion processes. The presence of water during HTC also contributes to the formation of highly regular and small-diameter particles, thus yielding products with better grindability properties than the ones produced from traditional thermochemical processes such as torrefaction or carbonization (Acharya et al., 2015; Kumar et al., 2018).

As of late, several studies have been conducted on HTC as a treatment for heterogeneous waste materials, such as MSW, with a focus on the fuel properties of hydrochars. For instance, Kim et al. (2017) observed that the properties of MSW and mixtures of newspaper and vegetables were significantly improved by the HTC process, yielding coal-like products. The authors reported that the hydrothermal treatment increased calorific value, fixed carbon and carbon contents of the feedstock and that the fuel properties of the obtained hydrochars were comparable to lignite and subbituminous coal. Berge et al. (2011) performed HTC of different feedstocks, including mixed MSW and evaluated the composition and fuel properties of the produced hydrochars. The authors indicated that approximately 49–75% of the initial carbon is retained in the hydrochar, 20–37% is transferred to the process water and 2–11% is recovered in the gas phase. These authors suggest that dehydration and decarboxylation are the governing reactions during HTC, resulting in hydrochars with greater carbon and lower oxygen concentrations, an improved HHV and a significant degree of aromaticity. Moreover, since different feedstocks and process parameters yield hydrochars with distinct properties, these solid products not only show potential for energy applications, but also as catalysts, soil ameliorants or adsorbents (Puccini et al., 2018).

Despite the positive features of the HTC process regarding hydrochar properties, the management or eventual valorization of the process water is one of the main challenges in scaling-up and making this process environmentally friendly. Besides being produced in significant amounts, this effluent contains high amounts of dissolved organic and inorganic compounds that should be removed before discharge. Recirculation of the process water after hydrochar filtration was studied by Stemann et al. (2013) and Catalkopru et al. (2017). Both works showed that this approach can increase hydrochar mass and energy yields. As such, characterization of HTC process water is important in selecting possible treatment options that may contribute to improve process sustainability.

The aim of this work was to assess the HTC process as an upgrading thermal technology for RDF containing miscellaneous polymeric waste with high contents of ash and chlorine, in order to obtain a solid fuel with appropriate characteristics for subsequent energy conversion processes, like combustion and gasification. The present work addresses for the first time the hydrothermal conversion of an industrial RDF, resulting from the mechanical treatment of industrial wastes and corresponding to what is designated as polymeric fraction.

For this purpose, characterization of the two major HTC products (hydrochar and process water) was performed. HTC tests were conducted by varying process parameters such as temperature, residence time and RDF-to-water mass ratio. The obtained products were characterized to evaluate the impact of these process parameters in their chemical composition, physical properties, and potential applications. Furthermore, process energetics was also estimated which is relevant for scaling-up purposes.

2. Materials and methods

2.1. Raw material

An industrial Refuse Derived Fuel (RDF) sample, produced via mechanical treatment, was supplied by CITRI, S.A. (Centro Integrado de Tratamento de Resíduos Industriais) a waste management company set in Setúbal, Portugal. RDF sampling was performed through the quartering technique, starting from a sample of 300 kg, and successive sample size reduction until a gross sample of 25 kg was reached. Prior to HTC experiments, the RDF gross sample was further grinded (DeLonghi mill) until it reached a fine form (<10 mm). Detailed composition of similar RDF samples can be found elsewhere (Nobre et al., 2019a, 2019b).

2.2. Hydrothermal carbonization experiments

HTC experiments were carried out using a 1 L stainless steel autoclave reactor (Parr Pressure Reactor) coupled with an electric heater and a PID controller (Parr 4848 Reactor controller), under autogenic pressure. For each experiment, approximately 20 g of RDF (as received) was added to the reactor with tap water (1:15 or 1:5 mass ratio). The reactor was sealed, put under vacuum, and heated to the desired carbonization temperatures (250, 275 and 300 °C). Then, the reactor was maintained at such temperatures for designated residence times (30 and 120 min). After reaction, the solid product (hydrochar) was washed with 1 L of deionized water and separated by filtration through a preweighted qualitative filter paper, air-dried for 12 h and oven-dried at 105 ± 2 °C for 12 h. After drying, the hydrochar samples were stored in air-tight containers until subsequent characterization analysis. The liquid product (process water) was stored at 4 °C until further analysis.

The hydrochar samples were coded with "H-X-Y/Z", where "X" represents operating temperature, "Y" represents residence time and "Z" represents RDF-to-water mass ratio. Process water samples from each experiment were identified by replacing the letter "H" by "W" and followed the same nomenclature. The layout of all the HTC experiments is described in Table S1 (Supplementary data).

2.3. Refuse derived fuel and hydrochar characterization

2.3.1. Chemical characterization and fuel properties

Prior to characterization analysis, RDF and hydrochars were milled (DeLongui mill) and sieved (Retsch) to a particle size diameter < 500 μm. All the determinations were conducted in triplicate, and the presented results correspond to average values.

Moisture, volatile matter and ash contents were determined according to standards EN 15414-3:2011, EN 15402:2011 and EN 15403:2011, respectively (European Standard, 2011a, 2011b, 2011c). Fixed carbon content was calculated by difference (in a dry basis, db). Elemental composition (C, H, N, S) was determined using an elemental analyzer (Thermo Finnigan – CE Instruments Model Flash EA 112 CHNS series). Oxygen content was calculated by difference (in a dry ash free basis, daf). Chlorine content was determined using X-Ray fluorescence analysis (Thermo Scientific Niton XL3t GOLDD+). High heating values (HHV) were determined with a bomb calorimeter (IKA C200) using benzoic acid as a calibration standard.

Mass and energy yields of the hydrochars (in a dry basis, db) were calculated using Eqs. (1) and (2), respectively:

$$Mass\ yield\ (\%, db) = \frac{m_{hydrochar}}{m_{RDF}} \times 100 \quad (1)$$

$$Energy\ yield\ (\%, db) = Mass\ yield \times \frac{HHV_{hydrochar}}{HHV_{RDF}} \quad (2)$$

where $m_{hydrochar}$ and $HHV_{hydrochar}$ are the mass and high heating value of hydrochar; m_{RDF} and HHV_{RDF} are the mass and high heating value of RDF. The energy yield is only focused on the amount of energy transferred from the raw RDF to the hydrochar.

Diehlorination efficiency was estimated according to Eq. (3), as described by Zhang et al. (2020):

$$Dechlorination\ efficiency(\%, db) = \left(1 - \frac{Cl_{hydrochar} \times Mass\ yield}{Cl_{RDF}}\right) \times 100 \quad (3)$$

where $Cl_{hydrochar}$ and Cl_{RDF} correspond to the chlorine content determined in the RDF and in the hydrochar, respectively.

2.3.2. Thermal and structural analysis

Thermal degradation profiles of RDF and hydrochars were assessed through thermogravimetric analysis using a thermogravimetric analyzer (TA Instruments, SDT 2960 Simultaneous DSC-TGA), from room temperature to 800 °C with a heating rate of 10 K/min, under air atmosphere, with an air flow of 100 mL/min.

Lorentzian multi-peak deconvolution was used to separate the overlapping peaks of the differential thermogravimetry (DTG) curves, assuming a symmetrical degradation pattern of the biomass components. The areas under DTG curves were considered proportional to the mass loss of the individual biomass components, allowing the calculation of the biomass composition. The Lorentzian function is defined according to the following equation:

$$y = \frac{y_0 + 2A/\pi \times w}{4 \times (T - T_c)^2 + w^2} \quad (4)$$

where A is peak area, T is temperature (°C), T_c is the central value of the peak and w is peak width.

The ignition and burnout temperatures were calculated using the intersection and conversion methods, respectively (Lu and Chen, 2015).

Morphological analysis was carried out on ground RDF and hydrochar samples through scanning electron microscopy (Nano-SEM, FEI Nova 200 (FEG/SEM)).

The functional groups on the surface of the RDF and hydrochar samples were identified by FT-IR. Infrared spectra (4000–650 cm^{-1}) were obtained based on the attenuated total reflectance (ATR) method using a FT-IR Spectrometer (Nicolet iS10, Thermo Scientific), equipped with a diamond ATR attachment by using 128 scans at a resolution of 4 cm^{-1}.

2.4. Process water characterization

The liquid fractions obtained in each HTC experiment were characterized for their pH, conductivity, chemical oxygen demand (COD), biochemical oxygen demand (BOD_5), total dissolved solids (volatile and fixed solids), Kjeldahl nitrogen, total phosphorous, total phenolic compounds and total reducing sugars. The determinations were carried out in triplicate, and the presented results correspond to average values.

pH was measured with a pH meter (Crimson MicropH 2001m). Electrical conductivity was measured by electrometric method (MC226 Conductivity meter Mettler Toledo). Chlorine content in the process water was determined by titration according to the methodology described in EPA- SW-948 test method 9253. BOD_5 quantification was performed following the OxiTop® methodology. Total phenolics were measured by the Folin-Ciocalteau method, with an adaptation of the method described by Singleton et al. (1998). Total reducing sugars content was determined through the dinitrosalicylic acid method (DNS) method, as proposed by Miller (1959). Total solids, Kjeldahl nitrogen, total phosphorous and COD were quantified according to methods 2540B, 4500N_{org}-C, 4500P-E and 5220B, respectively, from the Standard Methods for the Examination of Water and Wastewater.

Qualitative analysis of the organic fraction present in the process water was done as described in a previous work (Nobre et al., 2019a). Briefly, process water samples (5 mL) were acidified until pH 2 with 97% H_2SO_4 and were extracted three times with $CHCl_3$ (2 mL each extraction). The extracts were combined and dried with anhydrous sodium sulphate, filtered and derivatized with BSA (N, O-Bis(trimethylsilyl)acetamide). Finally, the extracts were injected in a GC-MS analyzer (Focus GC, Polaris Q - Thermo), equipped with a DB-5 capillary column (30 m length, 0.25 mm inner diameter and 0.25 μm film thickness). The extracts were injected in split mode, at 250 °C and the GC temperature was programmed in four stages: (i) initial temperature of 35 °C, held for 4 min; (ii) increased to 150 °C at a rate of 4 °C/min; (iii) increased to 280 °C at 10 °C/min; (iv) constant temperature of 280 °C held for 5 min. The transfer line and ion source temperatures were 270 °C and 200 °C, respectively. The organic profile of the chloroform extracts was determined by comparing the obtained mass spectra with those in NIST and WILEY databases.

2.5. Energy calculations

Energy calculations for the HTC process were based on the work of Mau and Gross (2018). Energy requirements (Q_{input}) were calculated according to Eq. (5):

$$Q_{input} = \frac{m_w(H_{w,HT} - H_{w,RT}) + m_{RDF}Cp_{RDF}\Delta T}{m_{RDF}} \quad (5)$$

where Q_{input} (MJ) is the energy input during the HTC process, m_w (kg) and m_{RDF} (kg) are the amounts of water and RDF. $H_{w,HT}$ and $H_{w,RT}$ (both in MJ/kg) are the enthalpy of water at the final hydrothermal temperature and at room temperature, respectively. Cp_{RDF} (MJ kg^{-1} K^{-1}) is the specific heat capacity of RDF, taken from a previous work (Nobre et al., 2019b). The evaluation of the energy input does not include a term corresponding to equipment heating or thermal losses. This is based on the assumption that these energy requirements might be compensated by the negative heat of reaction from the HTC process and energy recovery from the hydrochars (Cuvilas et al., 2015; Heidari et al., 2020)

The energy output (Q_{output}) of the process was calculated through Eq. (6):

$$Q_{output} = m_{hydrochar} \times HHV_{hydrochar} \quad (6)$$

where Q_{output} is expressed in MJ, $m_{hydrochar}$ (kg) is the mass of hydrochar, and $HHV_{hydrochar}$ (MJ/kg) is the HHV of hydrochar.

The net energy generation (Q_{net}) was estimated by Eq. (7):

$$Q_{net} = Q_{output} - Q_{input} \quad (7)$$

Process energy efficiency (PEE) was calculated according to Eq. (8):

$$PEE(\%) = \frac{Q_{output}}{(m_{RDF} \times HHV_{RDF}) + Q_{input}} \times 100 \quad (8)$$

3. Results and discussion

3.1. Proximate analysis, elemental analysis, and fuel properties

The HTC process had a clear effect on the visual aspect of the solid products regarding their homogeneity. The process converted RDF into a dark, friable, and uniform shaped hydrochar, as shown in Fig. S1 (Supplementary data). All the hydrochars were easily grinded when compared with the original RDF and the increase in sample brittleness was more pronounced for the hydrochars produced at 300 °C both at 30 and 120 min.

The results obtained for proximate analysis and ultimate analysis as well as for fuel properties of the original RDF and produced hydrochars are summarized in Table 1.

The hydrochars presented lower moisture contents between 0.5 and 1.4 wt%, after the drying stage. According to Lu et al. (2011), hydrolysis reactions occurring during HTC are responsible for the rupture of water bound to the raw material, which in conjunction with the improvement of hydrophobicity may contribute further for the reduced moisture contents. This is an important feature regarding storage of hydrochars, since reduced moisture and increased hydrophobicity are important factors in reducing microbial contamination, and moisture uptake upon exposure to atmospheric conditions (Kambo and Dutta, 2015a).

Proximate analysis showed that the HTC process caused a decrease in volatile matter present in hydrochars, when compared with raw RDF. This parameter was reduced from 85.1% to values between 79.6% and 82.7%, which can be explained by dehydration and decarboxylation reactions occurring during HTC (Toptas Tag et al., 2018). Changing RDF-to-water mass ratio from 1:15 to 1:5 caused an increase in volatile matter of the hydrochars from 78.6% to 80.4% possibly due to higher partition of degradation products to the hydrochars as the aqueous solution became saturated.

Increased temperatures and longer residence times showed a positive trend towards reduced ash contents of the hydrochars, showing values that varied from 3.3 to 5.3 wt%. These results corresponded to reductions of ash contents between 50.5 and 69.2%, when compared with the value present in the original RDF (10.7 wt%). Ash contents of the hydrochars obtained with a residence time of 120 min were slightly lower (3.3–4.3 wt%) than for hydrochars produced at the same temperature for 30 min (3.8–5.3 wt%), indicating that longer residence times may favor the dissolution of the mineral fraction in the aqueous phase. These reductions in inorganic content are mainly attributed to the solubility of those components in subcritical water conditions and have been reported by different authors using different raw materials such as *Miscanthus* × *giganteus* (Mihajlović et al., 2018) or TetraPak (Lokahita et al., 2017).

Given the trends observed for volatile matter and ash contents, the HTC process had a positive effect in fixed carbon content. This parameter increased from 4.2 wt% (RDF) to values between 13.4 and 16.9 wt% for the hydrochars. According to Lin et al. (2017), these variations in fixed carbon concentration are influenced by aromatization and repolymerization reactions occurring during HTC.

Regarding ultimate analysis (Table 1), it can be observed that the HTC process caused an increase in carbon content and a decrease in hydrogen and oxygen contents. This outcome is a result of the elimination of oxygenated products and dissolution of mineral components. Changing the RDF-to-water mass ratio from 1:15 to 1:5 increased carbon content of the hydrochars from 62.6 to 64.1 wt%. Sulphur was not detected in the original RDF or any of the hydrochars. Nitrogen concentration in the hydrochars presented minor increases when compared to the original RDF. This was more significant for the hydrochar obtained at 250 °C and 120 min, indicating that, unlike oxygen, nitrogen was not easily eliminated by rearrangement of the C-N bonds. Nitrogen content of samples H-275-30/15 (1.7 wt%) and H-275-30/5 (2.1 wt%) showed that reducing the amount of water in the reactor may lead to higher nitrogen retention in the hydrochar. According to Wang et al. (2018b) higher nitrogen concentrations in hydrochars from food waste can be attributed to enhancements of polymerization reactions and to absorption of nitrogen containing substances present in the reactive medium. The compositional changes associated with the HTC process can be further assessed by analyzing the changes in O/C and H/C atomic ratios as represented in the Van Krevelen diagram (Fig. 1).

The produced hydrochars presented significant reductions in O/C and H/C ratios when compared to the original RDF, showing that HTC promotes a clear fuel upgrading effect. The hydrochars had O/C ratios lower than 0.34, which are close to lignite (0.38). On the

Table 1
Chemical characteristics and fuel properties of RDF and hydrochars.

Parameter	Sample							
	RDF	H-250-30/15	H-275-30/15	H-275-30/5	H-300-30/15	H-250-120/15	H-275-120/15	H-300-120/15
Proximate analysis (wt.%, db[a])								
Moisture[b]	6.0	0.5	0.6	0.5	0.6	0.7	0.7	0.7
Volatile matter	85.1	81.8	80.5	80.4	82.7	79.6	80.6	79.8
Ash	10.7	4.8	4.7	5.3	3.8	4.1	4.3	3.3
Fixed carbon	4.2	13.4	14.8	14.3	13.5	16.3	15.1	16.9
Ultimate analysis (wt.%, daf[c])								
C	53.7	61.9	62.6	64.1	64.5	64.8	66.7	62.9
H	8.7	7.9	7.2	7.3	8.0	7.7	7.7	8.0
N	1.5	1.8	1.7	2.1	1.9	2.4	1.7	2.1
S	0.0	0.0	0.0	0.0	0.0	0.0	0.0	0.0
O	36.1	28.4	28.5	26.5	25.6	25.0	23.8	27.1
Fuel properties								
HHV (MJ/kg, db)	21.2	26.1	25.2	26.3	27.7	27.4	28.1	27.2
Mass yield (%, db)	–	49.2	49.3	53.7	45.2	53.6	51.6	47.6
Energy yield (%, db)	–	60.4	58.7	66.5	59.2	69.3	68.3	61.0
Cl (wt.%, db)	2.03	1.27	0.91	1.08	1.01	1.06	0.90	0.95
Dechlorination efficiency (%, db)	–	69.2	77.9	71.4	77.5	72.0	77.1	77.7

[a] Expressed in a wet basis wb,wt.%.
[b] db – dry basis.
[c] daf – dry ash free basis.

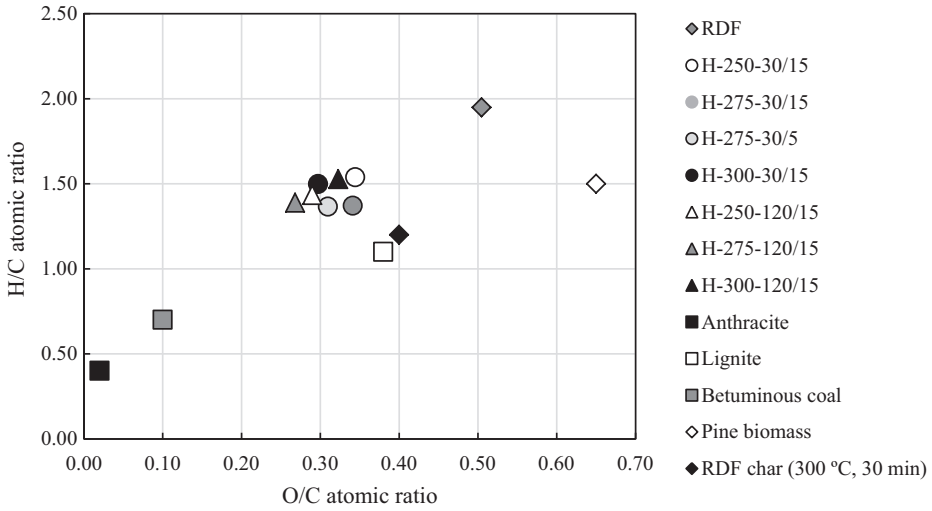

Fig. 1. Van Krevelen diagram comparing the produced hydrochars, RDF, biomass, fossil fuels (van der Stelt et al., 2011) and RDF char (Nobre et al., 2019b).

other hand, the H/C ratios were comparable to lignocellulosic biomass (from 1.37 to 1.54). This coalification effect is mostly related with dehydration and decarboxylation reactions (Kim et al., 2017).

Performance of the HTC process and fuel quality of the hydrochars were also assessed by parameters like HHV, dechlorination efficiency, mass and energy yields (Table 1).

The HTC process increased HHV values and decreased the chlorine content of the hydrochars when compared to the original RDF. The HHV of the hydrochars varied between 25.2 and 28.1 MJ/kg and were comparable with the HHV of lignite (25.7 MJ/kg) (Liu et al., 2013). Hydrochar yields generally decreased with temperature and increased with residence time, because higher temperatures favor decomposition and product dissolution in process water. In contrast, longer residence times could further enable the polymerization and cross-linking reactions leading to condensation of the HTC products, thus increasing hydrochar yield (Lin et al., 2017; Zhao et al., 2018). Positive correlations between hydrochar yield and residence time have been reported for HTC of food waste (Zhao et al., 2018) and pine biomass (Wu et al., 2017). According to Nakason et al. (2018), energy yield can be used to determine optimal HTC conditions, since it measures how much energy of the original raw material is retained in the hydrochar. The energy yields determined in this work follow the same tendency as the mass yields and HHV, that showed positive correlations with residence time. The highest energy yields (69.3% and 68.3%) were obtained for residence time of 120 min at the temperatures of 250 °C and 275 °C, respectively. Higher HTC temperatures may lead to further decomposition of the feedstock and shorter residence time limits the extent of condensation reactions. These factors can reduce carbon recovery in the solid products and consequently decrease energy yield (Kambo and Dutta, 2015).

The dechlorination efficiencies of the HTC process varied from 69.2% (H-250-30/15) to 77.9% (H-275-30/15). The decrease in chlorine content has also been reported for hydrochars produced from mixtures of medical wastes and lignocellulosic biomass (Shen et al., 2017), PVC (Poerschmann et al., 2015) and mixtures of bamboo and PVC (Yao and Ma, 2018). Changing the RDF-to-water mass ratio from 1:15 to 1:5 improved mass yield and the HHV of the hydrochars (therefore increasing energy yield) but it had a negative effect in dechlorination, decreasing this parameter from 77.9% to 71.4%. As a lower amount of water is available, a lower proportion of HTC degradation products are dissolved in the aqueous medium justifying the lower dechlorination efficiency. On the other hand, different authors indicated that higher amounts of water in the reactor enhance hydrolysis reactions, which can account for the higher mass yield found with H-275-30/5 (Oktaviananda et al., 2017; Román et al., 2012).

Generally speaking, the fuel properties of hydrochars were improved with the increase of residence time, since ash and chlorine contents were reduced while mass yield rose. Higher RDF-to-water ratio contributed to increase HHV and mass yield, but chlorine and ash contents were greater. Temperature seemed to have no direct correlation with the previous parameters, although it promoted a reduction of mass and energy yields. The hydrochar with the best fuel properties was H-275-120/15, presenting the highest HHV (28.1 MJ/kg db) and the lowest chlorine concentration (0.9 wt% db).

3.2. Thermal analysis

The results of thermal degradation of RDF and selected hydrochars during combustion are represented in Fig. 2.

The TGA profiles of RDF, H-250-30/15, H-300-30/15 and H-300-120/15 are very similar in shape, with two thermal decomposition stages, as determined by the multi-peak deconvolution. The first decomposition stage occurs at temperatures between 312 °C and 317 °C while the second stage occurs between 438 °C and 459 °C.

Biomass structural components, namely cellulose (250–350 °C), hemicellulose (200–300 °C) and lignin (200–500 °C), decompose in these two stages, and it is largely assumed that during combustion the mass loss obtained in these temperature intervals correspond to CO_2 and CH_4 release (Carrier et al., 2011; Mihajlović et al., 2018). It is safe to assume that the hemicellulose fraction was significantly lower for the produced hydrochars. The relative abundances of polysaccharide and lignin fractions might be approximated with Lorentzian multi-peak deconvolution (Fig. 2d). As can be seen from the Fig. 2d. as the HTC temperature and residence time increase, the relative polysaccharide fraction decreases and lignin fraction increases. This result highlights the effect of higher temperatures and residence times in hydrochar production, reinforcing the degree of molecular rearrangement and decomposition caused by the HTC process. As such, the greater mass loss found for the RDF sample can represent the oxidation of biomass main constituents and the presence of different volatile matter fractions (Sever Akdağ et al., 2016).

The ignition temperatures (Table S2, Supplementary data) did not change significantly among the samples (260 °C, 250 °C, 260 °C, 255 °C, for RDF, H-250–30/15,H-300–30/15, and H-300–

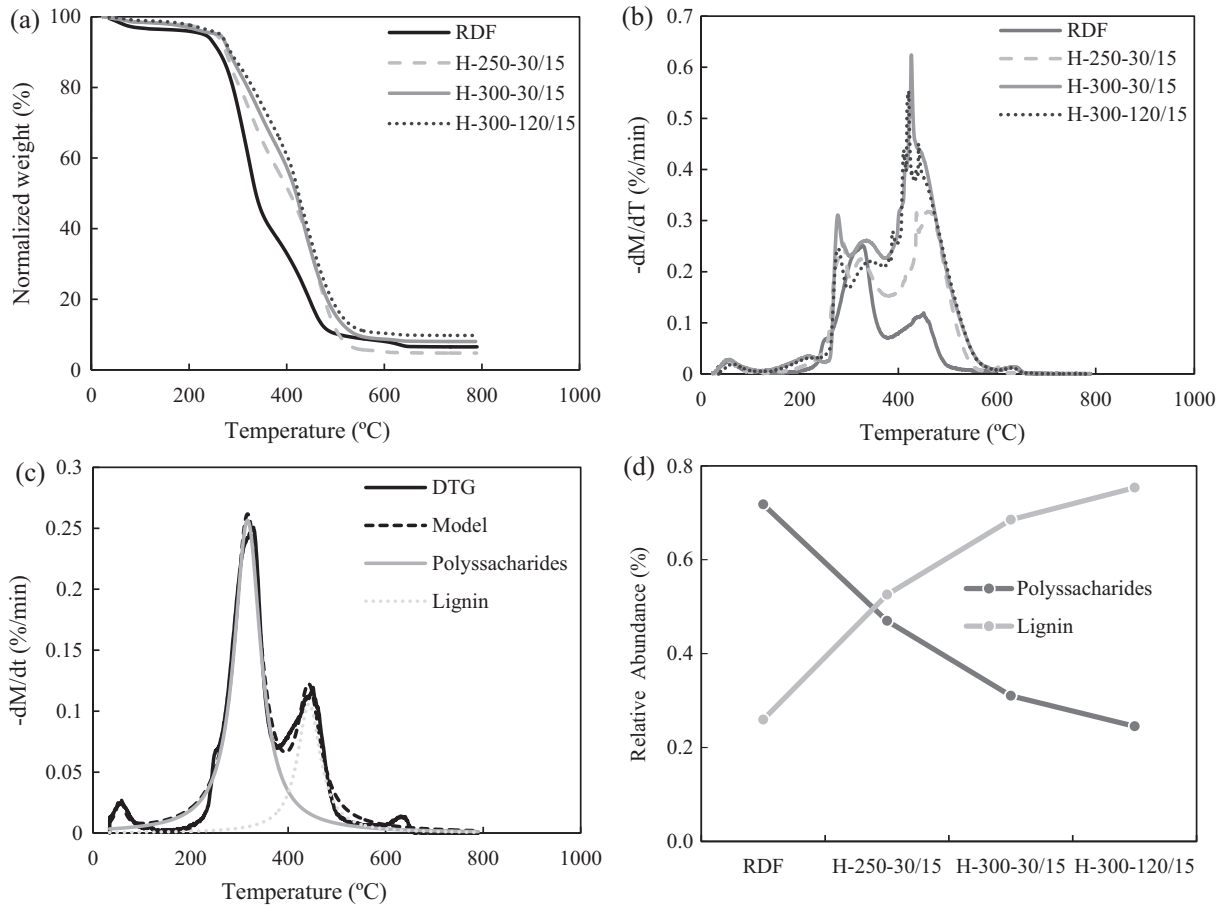

Fig. 2. (a) TGA curves; (b) DTG curves; (c) Deconvolution of RDF DTG curve; and (d) Relative abundance of the two main peaks (polyssacharides and lignin) for each studied sample.

120/15, respectively) possibly because of the low polysaccharide content of the RDF. On the other hand, burnout temperatures decreased significantly (623 °C, 556 °C, 576 °C and 576 °C, respectively for RDF, H-25-30/15, H-300-30/15, and H-300-120/15). The results indicate that the RDF and hydrochars have similar ignition properties and their ignition temperatures are lower than that of lignite. The lower burnout temperatures of hydrochars suggest that they can be burned in lower temperatures and in shorter residence times than RDF.

3.3. Structural properties

Microscopic observations of the RDF and the produced hydrochars revealed interesting morphological alterations brought by the HTC process. The SEM images of RDF and hydrochars H-250–30/15, H-300–30/15 and H-300–120/15 are presented in Fig.S2 (Supplementary data). The surface morphology of RDF was quite fibrous and smooth, denoting some rigidity. After HTC, substantial changes on the surface morphology could be perceived. One of the most apparent changes is related to the degradation of the fibrous structure into fragments with grooves and holes that were seen in the three hydrochar samples. Hydrochars presented a more disordered structure, particularly sample H-300-30/15 showing visible cracks that could be related with the release of volatile matter during the thermal process (Ma et al., 2016; Saqib et al., 2018).

The FT-IR analysis enabled further understanding on the structural composition, namely differences in functional groups between the original RDF and the hydrochars. FT-IR peak frequencies and respective assignments are presented in Table 2.

The peaks at 3295 and 3296 cm^{-1}, which are attributable to O-H stretching vibration in hydroxyl or carboxyl groups, were present in all samples but became weaker at increased temperature and residence times due to dehydration and decarboxylation reactions. This observation is in accordance with the results depicted in the Van Krevelen diagram (Fig. 1), and it can also mean a higher degree of hydrophobicity for the hydrochars, which is a very important feature regarding storage of solid fuels (Liu et al., 2013). C-H stretching of methyl, methylene and methine groups are reflected in peaks at 2914–2915 cm^{-1} and 2846–2848 cm^{-1}. These groups are present in hemicellulose, cellulose and lignin, and the peak intensity decreased for all hydrochar samples, particularly in samples H-300-30/15, H-275-120/15 and H-300-120/15. These samples represented the most severe HTC conditions and, as such, the first peak (2914-2915 cm^{-1}) is small, and at 2846–2848 cm^{-1} the peaks disappeared. This could be related with the more extensive oxidation of the biomass components occurring at these conditions. Peaks present at 1691–1692 cm^{-1} and 1585–1591 cm^{-1} were not detected in the RDF spectrum. These peaks correspond to C=O and C=C stretching in aromatic rings and became more intense with the increase in temperature and residence time. The hydrochar produced with a higher RDF-to-water mass ratio (1:5) also presented a greater peak intensity at these wavenumbers. The higher intensity of these peaks may be related with condensation and polymerization reactions that occur extensively for longer reaction times and with reduced water volume, reflecting on an increased mass yield obtained for samples H-275–30/5, H-250–120/15 and H-275–120/15.

Peaks corresponding to Aryl-O stretching in aromatic ethers (1248–1264 cm^{-1}) and C-O stretching in the hydroxyl group of phenolic compounds (1202–1206 cm^{-1}) increased with process

Table 2
FT-IR peak frequencies (cm^{-1}) and corresponding assignments for RDF and hydrochar samples.

Sample								Assignment
RDF	H-250-30	H-275-30	H-275-30/5	H-300-30	H-250-120	H-275-120	H-300-120	
3296	3295	3295	3295	3296	3295	3295	3296	O-H stretching in hydroxyl and carboxyl groups (Yao and Ma, 2018).
2914	2914	2915	2915	2915	2915	2915	2914	C-H stretching in aliphatic methyl, methylene and methine groups (Shen et al., 2017).
2846	2848	2848	2846		2847			
	1692	1692	1691	1691	1692	1691	1691	C=O stretching in quinone, conjugated ketone, amide or carboxylic acid (Wu et al., 2017) (Coates, 2000).
	1591	1596	1587	1587	1587	1587	1585	C=C stretching in aromatic rings (Kabadayi Catalkopru et al., 2017).
1443				1443		1443	1440	C-H bending in methyl group (Coates, 2000).
1264	1254	1251	1263	1263	1257	1264	1264	Aryl-O stretching in aromatic ethers (Stemann et al., 2013).
1206	1201	1206	1202	1202	1206	1206	1206	C-O stretching in phenolic hydroxyl group (Coates, 2000) (Yan et al., 2017).
	1107	1107	1099	1101	1109	1098	1095	C-O stretching in ethers (alkyl substituted or large cyclic ethers) or C-N stretching in primary amines (Coates, 2000).
	1031	1030	1030	1030	1031	1031	1029	
		781	782	781		782	782	C-H out-of-plane bending in aromatic rings (875–650 cm^{-1}) (Wu et al., 2017)
663	669	668	668	651	668	669	668	C-Cl stretching in aliphatic chloro compounds (800–600 cm^{-1}) (Shen et al., 2017)

temperature, and were more pronounced in samples H-275-30/15 and H-300-30/15. These peaks also showed a slight decrease for longer residence times, and they correspond to lignin interactions, which have a more complex degradation profile (Liu et al., 2013).

The decrease in chlorine content can also be related to the FT-IR data, since the peaks at 651–669 cm^{-1} were significantly smaller for the hydrochars when compared to the original RDF.

3.4. Process water characterization

HTC process water has been thoroughly described in the literature as one of the main drawbacks of this thermal conversion process, mostly due to its considerable amounts and heavy pollutant charge (Catalkopru et al., 2017). Results for the characterization of the process waters generated in each HTC experiment are presented in Table 3.

All process waters were acidic with pH values that ranged from 2.8 to 4.0. These values are likely due to the presence of organic acids formed by thermal decomposition of sugars present in the biomass fraction of the RDF (Becker et al., 2014; Berge et al., 2011). Temperature and residence time did not seem to exert significant effects on this parameter, whereas the RDF-to-water mass ratio of 1:5 was found to decrease pH probably due to the concentration effect of acidic components, since the amount of available water was lower. Furthermore, sample W-275-30/5 presented the highest conductivity (9.2 mS/cm) and fixed solids (6.7 g/L) values, which also establishes the impact of the RDF-to-water mass ratio in the concentration of inorganic species.

Nitrogen presented values between 26.1 mg/L and 49.2 mg/L, showing a tendency to decrease for higher temperatures. At 300 °C (30 and 120 min), nitrogen values in the process water were lower when compared with the greater nitrogen contents found in samples H-300-30/15 and H-300-120/15 (2.1 wt%). Although found in very small concentrations, total phosphorous revealed a decreased tendency with temperature and residence time. These results could arise from the reaction of phosphorous with metallic cations such as calcium, magnesium, aluminum or iron, resulting in precipitates that could be deposited in the surface of the hydrochars (Idowu et al., 2017). Reducing sugars concentration had a higher value at 250 °C for 30 min (6.7 g/L) but decreased for the subsequent temperatures, and for the tests conducted for 120 min. At higher temperatures, as well as longer residence times, the degradation of reducing sugars to yield organic acids and CO_2, justifies this decrease in their concentration in process waters (Wang et al., 2018b).

COD and BOD_5 of process waters showed a relation with all operating variables. These parameters increased with temperature, residence time and with the reduction in the amount of water added to the reactor. COD values varied between 12.2 gO_2/L (W-250-30/15) to 27.2 gO_2/L (W-275-30/5). Higher temperatures and longer residence times increased the degradation of the RDF, allowing the number of oxidizing compounds to increase. A reduced amount of water in the reactor, leads to a concentration effect reflected on a higher COD value of 27.2 gO_2/L. On the other hand, BOD_5 presented values between 300 and 450 mgO_2/L. These low values are indicative of poor biodegradability and can be related with the presence of aromatic hydrocarbons and phenolic

Table 3
Chemical characterization of the process waters obtained from the different HTC tests.

Parameter		Unit	Sample						
			W-250-30/15	W-275-30/15	W-275-30/5	W-300-30/15	W-250-120/15	W-275-120/15	W-300-120/15
pH		Sorensen	3.2	3.8	2.8	3.8	3.2	3.8	4.0
Conductivity		mS/cm	5.0	6.1	9.2	4.1	5.7	6.7	4.0
COD		gO_2/L	12.2	12.8	27.2	13.8	12.7	14.2	15.5
BOD_5		mgO_2/L	300	333	450	350	333	393	400
Solids	Total	g/L	12.2	11.7	23.1	12.5	11.2	10.8	13.5
	Fixed		3.6	3.2	6.7	3.9	3.8	3.4	3.9
	Volatile		8.6	8.6	16.4	8.7	7.4	7.4	9.6
Kjeldahl nitrogen		mg/L	41.7	42.9	49.2	30.5	41.1	44.8	26.1
Total phosphorous			0.293	0.104	0.306	0.095	0.163	0.086	0.062
Total reducing sugars		g/L	6.7	4.2	5.1	5.1	4.7	4.8	4.3
Total phenolics			1.6	2.1	2.1	1.7	1.5	1.3	1.5
Chlorine			0.9	1.8	3.2	1.4	1.7	2.6	1.9

compounds (with values between 1.3 and 2.1 g/L) that are generally toxic to microorganisms. Since the BOD_5/COD values ranged from 0.02 to 0.03 the biological treatment of these process waters may not be a viable solution (Berge et al., 2011). COD and BOD values found for these process waters are significantly lower than values found for HTC of mixed MSW (Berge et al., 2011). RDF, as opposed to MSW, represents an already treated solid waste, meaning that during its production the organic and putrescible fraction is separated, leaving mostly lignocellulosic components and plastics, which could be the reason for lower COD and BOD values.

The nature of the organic compounds present in the process water samples was studied by GC-MS (Table 4), to clarify which were the main functional groups present in the process waters.

Temperature and residence time affected the distribution and variety of organic compounds found in the HTC process waters, and samples W-300-30/15 and W-300-120/15 presented the largest number of identifiable compounds, due to the more extensive degradation occurring at this temperature. Several acids, alcohols, ketones, aromatic hydrocarbons and phenolic compounds were identified with a cut-off value for relative peak area of 0.5%. Acetic, propionic and sorbic acids, as well as 3-furaldehyde and phenol were present in all the samples, at variable relative percentages. Similar organic contaminants were found in the process waters obtained from HTC of different waste materials like MSW or lignocellulosic biomass (Berge et al., 2011; Mihajlović et al., 2018).

The wide variety of aromatic compounds found in these process waters is consistent with other findings on RDF thermal conversion. According to Efika et al. (2015), there was a predominance of aromatic compounds in oil from RDF pyrolysis at 350 °C, as a result of their formation by conversion of alkanes to alkenes and subsequent Diels-Alder reactions, that are favored by high temperature and long residence times. Moreover, the presence of aromatic compounds, particularly polycyclic aromatic hydrocarbons (PAH) is an indicator of the toxicity and pollution potential of these process waters (Mihajlović et al., 2018). This is corroborated by the low biodegradability expressed through the BOD_5/COD values.

The role of the process water during the HTC process is complex and multifactorial because it constitutes a liquid medium for dissolution of multiple components of the raw materials and of newly formed products, it also acts as a reactive agent participating in the decomposition of the raw materials (Hori et al., 2019) and is the source of the autogenous pressure of the process. In that sense, the RDF-to-water mass ratio is a key parameter for the process efficiency and the final composition of the aqueous effluent.

Given the chemical characteristics of these samples, a detailed study on different solutions for the management of HTC process water is required. Process water recirculation, or extraction of added-value organic compounds may represent solutions to increase the sustainability of the HTC process by reducing the environmental impact of process waters.

Table 4
Qualitative analysis of the process water extracts by GC-MS.

Compounds	Molecular formula	Relative peak area (%)						
		W-250-30/15	W-275-30/15	W-275-30/5	W-300-30/15	W-250-120/15	W-275-120/15	W-300-120/15
Acetic acid	$C_2H_4O_2$	5.1	2.7	8.4	8.2	9.9	7.7	5.3
Prop-2-enoic acid	$C_3H_4O_2$		0.5		0.5		0.7	0.7
Propionic acid	$C_3H_6O_2$	1.0	0.6	1.5	1.4	1.0	1.7	1.2
Isobutyric acid	$C_4H_8O_2$			1.8	1.1		2.3	1.2
Sorbic acid	$C_6H_8O_2$	1.9	3.2	3.1	4.1	3.9	5.2	3.4
Benzoic acid	$C_7H_6O_2$				1.3			7.1
3-Methoxybenzoic acid	$C_8H_8O_3$	3.6	1.9		1.4	3.6		
1,2-Ethanediol	$C_2H_6O_2$				0.5			
Butanol	$C_4H_{10}O$			1.2	2.7		0.7	1.2
Pentanol	$C_5H_{12}O$							2.2
Octanol	$C_8H_{18}O$			4.7	4.5			
3-Furaldehyde	$C_5H_4O_2$	19.8	1.8	4.5	2.2	1.6	4	0.3
2,4-Dimethylfuran	C_6H_8O		0.7	3.9	1.7		2.6	2.3
3-Furaldehyde	$C_5H_4O_2$	19.8	1.8	4.5	2.2	1.6	4.0	0.3
2,4-Dimethylfuran	C_6H_8O		0.7	3.9	1.7		2.6	2.3
3-Hydroxybut-3-en-2-one	$C_4H_6O_2$							0.9
2-Methylcyclopent-2-en-1-one	C_6H_8O							11.3
1-(cyclohexen-1-yl)-ethanone	$C_8H_{12}O$		1.3		1.3			0.4
(2-hydroxyphenyl)-phenylmethanone	$C_{13}H_{10}O_2$		1.1	2.8			1.6	1.9
1-Phenylethanone	C_8H_8O							0.9
1-Phenanthren-9-ylethanone	$C_{16}H_{12}O$							1.2
3-Methoxybenzaldehyde	$C_8H_8O_2$		1.9	3.7	2.2			0.7
1-Phenoxynaphtalene	$C_{16}H_{12}O$	8.5		1.8		8.5	1.2	
Phenol	C_6H_6O	1.3	15.3	4.3	2.8	6.9	5.4	4.8
Benzene-1,4-diol	$C_6H_6O_2$			1.8				0.9
4-Methylphenol	C_7H_8O	1.9	1.6		1.4	1.9	4.5	2.0
2-Methylphenol	C_7H_8O	1.8				1.8	1.8	0.6
2-Methoxyphenol	$C_7H_8O_2$		0.8					3.1
2,6-Dimethoxyphenol	$C_8H_{10}O_3$			3.7				1.0
1,3,5-Trimethoxy-2-methylbenzene	$C_{10}H_{14}O_3$						1.2	1.0
2-Ethenyl-1,3,4,5-tetramethoxybenzene	$C_{12}H_{16}O_4$							1.0
2-Benzylphenol	$C_{13}H_{12}O$				12		1.4	1.2
1-Benzyl-2,4-dimethylbenzene	$C_{15}H_{16}$							0.6
1-Ethyl-2-methylphenanthrene	$C_{17}H_{16}$							0.5
4-[1-(3,4-dimethylphenyl)ethyl]-1,2-dimethylbenzene	$C_{18}H_{22}$		0.8					1.3
2,2,7,7-Tetramethyloctane	$C_{12}H_{26}$			1.2	0.8		1.2	0.5
Total identified peaks (%)		**44.9**	**34.2**	**48.4**	**50.1**	**39.1**	**43.2**	**60.7**

3.5. Energy calculations

Evaluation of energy balance of the HTC process was done by calculating the energy supplied to the process (Q_{input}) and the energy recovered from its products (Q_{output}). The heat requirements (Q_{input}) were calculated without accounting for thermal losses. The energy required to heat RDF during HTC does not account for water vaporization enthalpy because phase change is avoided in this process. Drying of the sample and obtained hydrochar were not considered in these calculations. Evaporation of water from the liquid phase was also not accounted for, since this phase is expected to be remediated or valorized (Kambo et al.,

Table 5
Energy calculations for RDF hydrothermal carbonization.

Process conditions			Energy calculations					
T (°C)	RDF-to-water mass ratio	t (min)	Hydrochar yield (%)	$Cp_{,RDF}$ (MJ kg^{-1} K^{-1})	Q_{input} (MJ)	Q_{output} (MJ)	Q_{net} (MJ)	PEE (%)
250	1:15	30	49.2	1.5×10^{-3}	14.45	12.81	−1.64	35.9
275	1:15	30	49.3		16.06	12.43	−3.62	33.4
275	1:5	30	53.7		5.60	14.10	8.50	52.6
300	1:15	30	45.2		17.67	12.55	−5.11	32.3
250	1:15	120	53.6		14.45	14.70	0.24	41.2
275	1:15	120	51.6		16.06	14.48	−1.58	38.9
300	1:15	120	47.6		17.67	12.93	−4.73	33.3

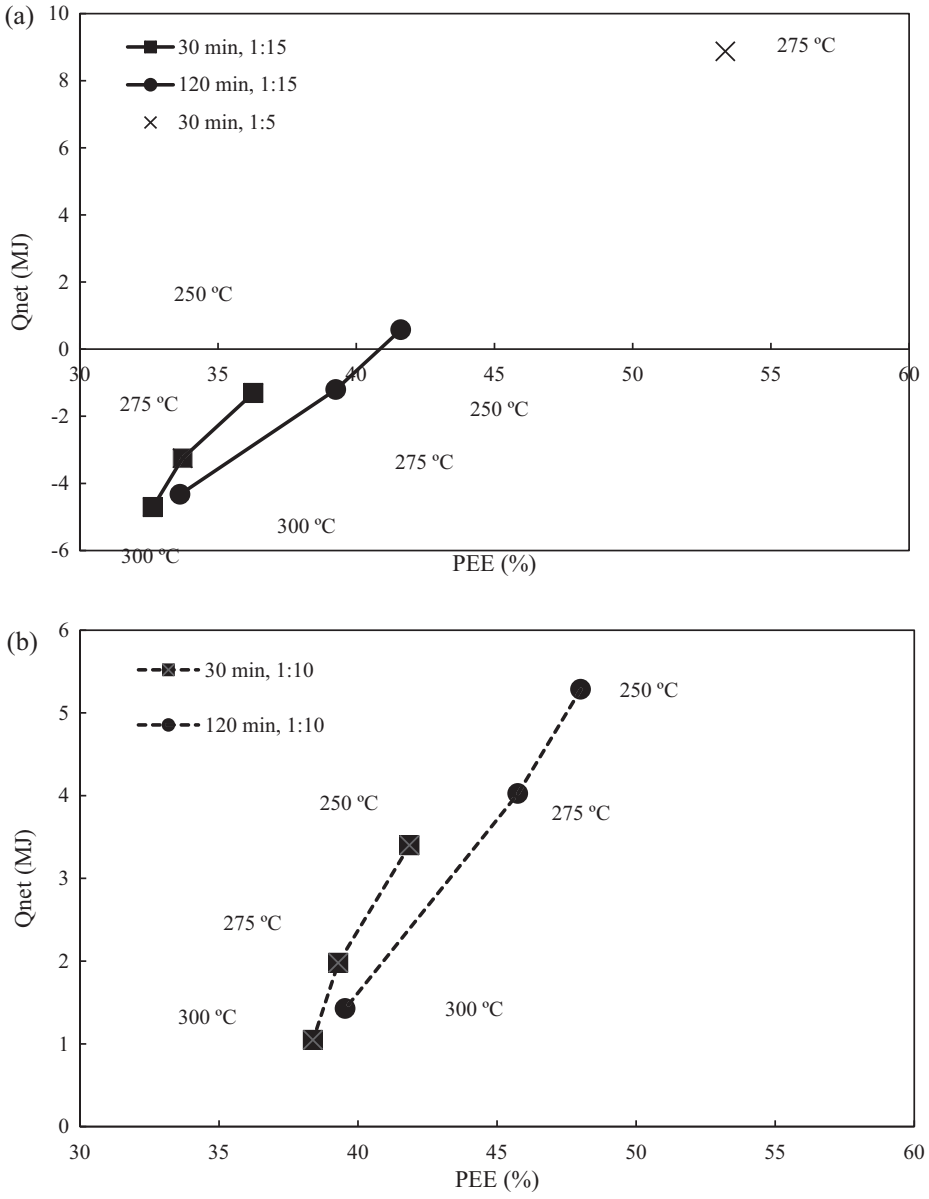

Fig. 3. Relation between PEE (%) and Q_{net} (MJ): (a) Results obtained in this work with RDF-to-water mass ratios of 1:15 and 1:5; (b) Calculations made for a projected RDF-to-water mass ratio of 1:10.

2018; Stemann et al., 2013). Furthermore, Q_{output} considers only the energy content of the hydrochar, since for each test, after reaching ambient pressure, gas formation was not relevant. Results for the energy calculations are presented in Table 5.

As expected, input energy increased with the increase of HTC temperature, but the RDF-to-water mass ratio played a major role in Q_{input} values. The lower Q_{input} value corresponds to HTC at 275 °C with a ratio of 1:5, meaning there is a smaller amount of water to heat. Considering 1 kg of RDF and 15 kg of water, the amount of energy required for the process, for all temperatures is always very high, and above 14.45 MJ. Meanwhile, partially due to the decline in hydrochar yield, Q_{output} decreased with increasing HTC temperature. The amount of water and the obtained hydrochar yields are reflected in the calculated Q_{net} values, and this parameter has positive values for the conditions with higher hydrochar yields. When compared with conventional RDF torrefaction or carbonization, HTC showed lower char yields, and requires further energy to heat water, thus presenting lower process efficiencies (Nobre et al., 2019b). The highest PEE value was obtained for the test with the RDF-to-water mass ratio of 1:5 (52.6%). These results suggest that HTC applied to RDF should be done with less water in the reactor, to minimize energy expenditure regarding water heating and also to obtain higher hydrochar yields. On the other hand, hydrochar fuel properties, namely HHV, did not present significant alterations regarding the use of different temperatures, residence times and RDF-to-water mass ratios. As such, taking into account the similar fuel properties obtained at the tested process conditions, a comparison between the obtained results and calculations made for a RDF-to-water mass ratio of 1:10 is represented in Fig. 3.

As expected, lowering the amount of water has a very positive effect on Q_{net} values and PEE (%). According to Missaoui et al. (2017), Q_{net} net values were negative (-2.4 MJ/kg) for a biomass-to-water ratio of 1:6, whereas for a ratio of 1:5 this parameter was positive (2.2 MJ/kg). Nevertheless, the low density of the RDF is an obstacle, since HTC requires the feedstock to be covered in water. Possibly, further reducing particle size of the RDF prior to HTC could help decrease the volume that this feedstock occupies in the reactor. On the other hand, less water also means the process water will have higher concentrations of several parameters, such as total solids content, fixed solids content, COD, Kjeldahl nitrogen, total phosphorous or chlorine, as previously discussed (Table 3). Optimization of this process is fundamental to further proceed to a larger scale, namely by testing different RDF particle sizes and RDF-to-water mass ratios. Furthermore, mixing RDF with other wastes, such as waste oils or waste animal fats, could also be positive regarding density of the sample and increasing hydrochar yield.

4. Conclusions

Hydrothermal carbonization of RDF between 250 °C and 300 °C, with residence times of 30 min and 120 min, and RDF-to-water mass ratios of 1:15 and 1:5, can be an effective way to upgrade this heterogeneous waste derived fuel. Increase in reaction temperature (up to 275 °C) and time (120 min) led to higher reaction severity, resulting in an increase in RDF degradation, polymerization and condensation of dissolved products resulting in higher mass yield. The produced hydrochars presented upgraded fuel properties, namely reduced volatile matter and ash contents as well as increased fixed carbon and HHV. The hydrochars showed similarities with fossil fuels such as lignite regarding reduced oxygen and hydrogen concentrations. These new-found characteristics illustrate their potential as alternative solid fuels. The process waters from all the HTC tests presented acidic pH and significant COD, high total phenolic and total reducing sugars values, as well as the presence of various organic species, namely organic acids, alcohols, furan derivatives, phenolic compounds and aromatic hydrocarbons. Owning to their composition, these process waters need further study to establish the best management practices and to increase sustainability of the HTC process.

Additionally, process energy efficiency can be improved by lowering the amount of water used in the process and by applying process conditions that optimize hydrochar mass yield, namely lower temperature, and longer residence time.

Declaration of Competing Interest

The authors declare that they have no known competing financial interests or personal relationships that could have appeared to influence the work reported in this paper.

Acknowledgments

This work was supported by the CITRI, S.A. project I&DT n° 24878. And by FCT - Fundação para a Ciência e Tecnologia, through grant SFRH/BD/111956/2015 and within the R&D Units Project Scope UIDP/04077/2020.

Appendix A. Supplementary data

Supplementary data to this article can be found online at https://doi.org/10.1016/j.wasman.2020.11.040.

References

Acharya, B., Dutta, A., Minaret, J., 2015. Review on comparative study of dry and wet torrefaction. Sustain. Energy Technol. Assess. 12, 26–37. https://doi.org/10.1016/j.seta.2015.08.003.

Lokahita, Baskoro, Aziz, Muhammad, Yoshikawa, K., Takahashi, F., 2017. Energy and resource recovery from Tetra Pak waste using hydrothermal treatment. Appl. Energy 207, 107–113. https://doi.org/10.1016/j.apenergy.2017.05.141.

Becker, R., Dorgerloh, U., Paulke, E., Mumme, J., Nehls, I., 2014. Hydrothermal carbonization of biomass: major organic components of the aqueous phase. Chem. Eng. Technol. 37, 511–518. https://doi.org/10.1002/ceat.201300401.

Berge, N.D., Ro, K.S., Mao, J., Flora, J.R.V., Chappell, M.A., Bae, S., 2011. Hydrothermal carbonization of municipal waste streams. Environ. Sci. Technol. 45, 5696–5703. https://doi.org/10.1021/es2004528.

Carrier, M., Loppinet-Serani, A., Denux, D., Lasnier, J.M., Ham-Pichavant, F., Cansell, F., Aymonier, C., 2011. Thermogravimetric analysis as a new method to determine the lignocellulosic composition of biomass. Biomass Bioenergy 35, 298–307. https://doi.org/10.1016/j.biombioe.2010.08.067.

Coates, J., 2000. Interpretation of infrared SpectraA practical approach. Encycl. Anal. Chem. https://doi.org/10.1002/9780470027318.

Cuvilas, C.A., Kantarelis, E., Yang, W., 2015. The impact of a mild sub-critical hydrothermal carbonization pretreatment on Umbila wood. A mass and energy balance perspective. Energies 8, 2165–2175. https://doi.org/10.3390/en8032165.

Efika, E.C., Onwudili, J.A., Williams, P.T., 2015. Products from the high temperature pyrolysis of RDF at slow and rapid heating rates. J. Anal. Appl. Pyrol. 112, 14–22. https://doi.org/10.1016/j.jaap.2015.01.004.

EN 15414-3 – Solid recovered fuels – Determination of moisture content using the oven dry method. Part 3: Moisture in general analysis sample.

EN 15402 – Solid recovered fuels – Determination of the content of volatile matter.

EN 15403 – Solid recovered fuels. Determination of ash content.

Heidari, M., Salaudeen, S.A., Arku, P., Acharya, B., Tasnim, S.H., Dutta, A., 2020. Development of a mathematical model for hydrothermal carbonization of biomass: comparison of experimental measurements with model predictions. Under Rev. J. Energy 214,. https://doi.org/10.1016/j.energy.2020.119020 119020.

Hori, H., Kakizawa, T., Kuriyama, N., Kabuki, A., Otsuki, M., Horii, Y., 2019. Decomposition of environmentally persistent cyclic methylsiloxanes in subcritical water. Sustain. Chem. Pharm. 13,. https://doi.org/10.1016/j.scp.2019.100160 100160.

Idowu, I., Li, L., Flora, J.R.V., Pellechia, P.J., Darko, S.A., Ro, K.S., Berge, N.D., 2017. Hydrothermal carbonization of food waste for nutrient recovery and reuse. Waste Manage. 69, 480–491. https://doi.org/10.1016/j.wasman.2017.08.051.

Kabadayi Catalkopru, A., Kantarli, I.C., Yanik, J., 2017. Effects of spent liquor recirculation in hydrothermal carbonization. Bioresour. Technol. 226, 89–93. https://doi.org/10.1016/j.biortech.2016.12.015.

Kambo, H.S., Dutta, A., 2015a. A comparative review of biochar and hydrochar in terms of production, physico-chemical properties and applications. Renew. Sustain. Energy Rev. 45, 359–378. https://doi.org/10.1016/j.rser.2015.01.050.
Kambo, H.S., Dutta, A., 2015b. Comparative evaluation of torrefaction and hydrothermal carbonization of lignocellulosic biomass for the production of solid biofuel. Energy Convers. Manage. 105, 746–755. https://doi.org/10.1016/j.enconman.2015.08.031.
Kambo, H.S., Minaret, J., Dutta, A., 2018. Process water from the hydrothermal carbonization of biomass: a waste or a valuable product?. Waste Biomass Valorization 9, 1181–1189. https://doi.org/10.1007/s12649-017-9914-0.
Kim, D., Park, K.Y., Yoshikawa, K., 2017. Conversion of municipal solid wastes into biochar through hydrothermal carbonization. Appl. Biochar Eng. https://doi.org/10.5772/intechopen.68221.
Kobayashi, J., Kawamoto, K., Fukushima, R., Tanaka, S., 2011. Woody biomass and RPF gasification using reforming catalyst and calcium oxide. Chemosphere 83, 1273–1278. https://doi.org/10.1016/j.chemosphere.2011.03.010.
Krysanova, K., Krylova, A., Zaichenko, V., 2019. Properties of biochar obtained by hydrothermal carbonization and torrefaction of peat. Fuel 256, 115929. https://doi.org/10.1016/j.fuel.2019.115929.
Kumar, M., Olajire Oyedun, A., Kumar, A., 2018. A review on the current status of various hydrothermal technologies on biomass feedstock. Renew. Sustain. Energy Rev. 81, 1742–1770. https://doi.org/10.1016/j.rser.2017.05.270.
Li, L., Diederick, R., Flora, J.R.V., Berge, N.D., 2013. Hydrothermal carbonization of food waste and associated packaging materials for energy source generation. Waste Manage. 33, 2478–2492. https://doi.org/10.1016/j.wasman.2013.05.025.
Lin, Y., Ma, X., Peng, X., Yu, Z., 2017. Hydrothermal carbonization of typical components of municipal solid waste for deriving hydrochars and their combustion behavior. Bioresour. Technol. 243, 539–547. https://doi.org/10.1016/j.biortech.2017.06.117.
Liu, Z., Quek, A., Kent Hoekman, S., Balasubramanian, R., 2013. Production of solid biochar fuel from waste biomass by hydrothermal carbonization. Fuel 103, 943–949. https://doi.org/10.1016/j.fuel.2012.07.069.
Lu, J.J., Chen, W.H., 2015. Investigation on the ignition and burnout temperatures of bamboo and sugarcane bagasse by thermogravimetric analysis. Appl. Energy 160, 49–57. https://doi.org/10.1016/j.apenergy.2015.09.026.
Lu, L., Namioka, T., Yoshikawa, K., 2011. Effects of hydrothermal treatment on characteristics and combustion behaviors of municipal solid wastes. Appl. Energy 88, 3659–3664. https://doi.org/10.1016/j.apenergy.2011.04.022.
Ma, W., Hoffmann, G., Schirmer, M., Chen, G., Rotter, V.S., 2010. Chlorine characterization and thermal behavior in MSW and RDF. J. Hazard. Mater. 178, 489–498. https://doi.org/10.1016/j.jhazmat.2010.01.108.
Ma, X., Zhou, B., Budai, A., Jeng, A., Hao, X., Wei, D., Zhang, Y., Rasse, D., 2016. Study of biochar properties by scanning electron microscope – energy dispersive X-Ray spectroscopy (SEM-EDX). Commun. Soil Sci. Plant Anal. 47, 593–601. https://doi.org/10.1080/00103624.2016.1146742.
Mau, V., Gross, A., 2018. Energy conversion and gas emissions from production and combustion of poultry-litter-derived hydrochar and biochar. Appl. Energy 213, 510–519. https://doi.org/10.1016/j.apenergy.2017.11.033.
Mihajlović, M., Petrović, J., Maletić, S., Isakovski, M.K., Stojanović, M., Lopičić, Z., Trifunović, S., 2018. Hydrothermal carbonization of Miscanthus × giganteus: structural and fuel properties of hydrochars and organic profile with the ecotoxicological assessment of the liquid phase. Energy Convers. Manage. 159, 254–263. https://doi.org/10.1016/j.enconman.2018.01.003.
Miller, G.L., 1959. Use of dinitrosalicylic acid reagent for determination of reducing sugar. Anal. Chem. 31, 426–428. https://doi.org/10.1021/ac60147a030.
Missaoui, A., Bostyn, S., Belandria, V., Sarh, B., Gökalp, I., 2017. Assessing the heat and energy balances of hydrochar production via hydrothermal carbonization of olive pomace. Eur. Biomass Conf. Exhib. Proc. 2017, 1393–1398.
Mohammed, I.S., Na, R., Kushima, K., Shimizu, N., 2020. Investigating the effect of processing parameters on the products of hydrothermal carbonization of corn stover. Sustainability 12. https://doi.org/10.3390/su12125100.
Nakason, K., Panyapinyopol, B., Kanokkantapong, V., Viriya-empikul, N., Kraithong, W., Pavasant, P., 2018. Hydrothermal carbonization of unwanted biomass materials: effect of process temperature and retention time on hydrochar and liquid fraction. J. Energy Inst. 91, 786–796. https://doi.org/10.1016/j.joei.2017.05.002.
Násner, A.M.L., Lora, E.E.S., Palacio, J.C.E., Rocha, M.H., Restrepo, J.C., Venturini, O.J., Ratner, A., 2017. Refuse Derived Fuel (RDF) production and gasification in a pilot plant integrated with an Otto cycle ICE through Aspen plus™ modelling: thermodynamic and economic viability. Waste Manage. 69, 187–201. https://doi.org/10.1016/j.wasman.2017.08.006.
Nobre, C., Alves, O., Longo, A., Vilarinho, C., Gonçalves, M., 2019a. Torrefaction and carbonization of refuse derived fuel: char characterization and evaluation of gaseous and liquid emissions. Bioresour. Technol. 285. https://doi.org/10.1016/j.biortech.2019.121325.
Nobre, C., Vilarinho, C., Alves, O., Mendes, B., Gonçalves, M., 2019b. Upgrading of refuse derived fuel through torrefaction and carbonization: evaluation of RDF char fuel properties. Energy 181. https://doi.org/10.1016/j.energy.2019.05.105.
Oktaviananda, C., Rahmawati, R.F., Prasetya, A., Purnomo, C.W., Yuliansyah, A.T., Cahyono, R.B., 2017. Effect of temperature and biomass-water ratio to yield and product characteristics of hydrothermal treatment of biomass. AIP Conf. Proc. 1823, 1–7. https://doi.org/10.1063/1.4978102.
Poerschmann, J., Weiner, B., Woszidlo, S., Koehler, R., Kopinke, F.D., 2015. Hydrothermal carbonization of poly(vinyl chloride). Chemosphere 119, 682–689. https://doi.org/10.1016/j.chemosphere.2014.07.058.
Puccini, M., Ceccarini, L., Antichi, D., Seggiani, M., Tavarini, S., Latorre, M.H., Vitolo, S., 2018. Hydrothermal carbonization of municipal woody and herbaceous prunings: Hydrochar valorisation as soil amendment and growth medium for horticulture. Sustain. 10. https://doi.org/10.3390/su10030846.
Reza, B., Soltani, A., Ruparathna, R., Sadiq, R., Hewage, K., 2013. Environmental and economic aspects of production and utilization of RDF as alternative fuel in cement plants: a case study of Metro Vancouver Waste Management. Resour. Conserv. Recycl. 81, 105–114. https://doi.org/10.1016/j.resconrec.2013.10.009.
Román, S., Nabais, J.M.V., Laginhas, C., Ledesma, B., González, J.F., 2012. Hydrothermal carbonization as an effective way of densifying the energy content of biomass. Fuel Process. Technol. 103, 78–83. https://doi.org/10.1016/j.fuproc.2011.11.009.
Saqib, N.U., Baroutian, S., Sarmah, A.K., 2018. Physicochemical, structural and combustion characterization of food waste hydrochar obtained by hydrothermal carbonization. Bioresour. Technol. 266, 357–363. https://doi.org/10.1016/j.biortech.2018.06.112.
Sever Akdağ, A., Atimtay, A., Sanin, F.D., 2016. Comparison of fuel value and combustion characteristics of two different RDF samples. Waste Manage. 47, 217–224. https://doi.org/10.1016/j.wasman.2015.08.037.
Shen, Y., Yu, S., Ge, S., Chen, X., Ge, X., Chen, M., 2017. Hydrothermal carbonization of medical wastes and lignocellulosic biomass for solid fuel production from lab-scale to pilot-scale. Energy 118, 312–323. https://doi.org/10.1016/j.energy.2016.12.047.
Silva, R.B., Fragoso, R., Sanches, C., Costa, M., Martins-Dias, S., 2014. Which chlorine ions are currently being quantified as total chlorine on solid alternative fuels?. Fuel Process Technol. 128, 61–67. https://doi.org/10.1016/j.fuproc.2014.07.003.
Singleton, V.L., Orthofer, R., Lamuela-Raventós, R.M., 1998. Analysis of total phenols and other oxidation substrates and antioxidants by means of folin-ciocalteu reagent. Methods Enzymol. 299, 152–178. https://doi.org/10.1016/S0076-6879(99)99017-1.
Stemann, J., Putschew, A., Ziegler, F., 2013. Hydrothermal carbonization: process water characterization and effects of water recirculation. Bioresour. Technol. 143, 139–146. https://doi.org/10.1016/j.biortech.2013.05.098.
Toptas Tag, A., Duman, G., Yanik, J., 2018. Influences of feedstock type and process variables on hydrochar properties. Bioresour. Technol. 250, 337–344. https://doi.org/10.1016/j.biortech.2017.11.058.
van der Stelt, M., Gerhauser, H., Kiel, J., Ptasinski, K., 2011. Biomass upgrading by torrefaction for the production of biofuels: a review. Biomass Bioenergy 35, 3748–3762. https://doi.org/10.1016/j.biombioe.2011.06.023.
Wang, G., Zhang, J., Lee, J.Y., Mao, X., Ye, L., Xu, W., Ning, X., Zhang, N., Teng, H., Wang, C., 2020. Hydrothermal carbonization of maize straw for hydrochar production and its injection for blast furnace. Appl. Energy 266, 114818. https://doi.org/10.1016/j.apenergy.2020.114818.
Wang, T., Zhai, Y., Zhu, Y., Li, C., Zeng, G., 2018a. A review of the hydrothermal carbonization of biomass waste for hydrochar formation: process conditions, fundamentals, and physicochemical properties. Renew. Sustain. Energy Rev. 90, 223–247. https://doi.org/10.1016/j.rser.2018.03.071.
Wang, Tengfei, Zhai, Y., Zhu, Y., Peng, C., Xu, B., Wang, Tao, Li, C., Zeng, G., 2018b. Influence of temperature on nitrogen fate during hydrothermal carbonization of food waste. Bioresour. Technol. 247, 182–189. https://doi.org/10.1016/j.biortech.2017.09.076.
Wilk, M., Magdziarz, A., Kalemba-Rec, I., Szymańska-Chargot, M., 2020. Upgrading of green waste into carbon-rich solid biofuel by hydrothermal carbonization: the effect of process parameters on hydrochar derived from acacia. Energy 202. https://doi.org/10.1016/j.energy.2020.117717.
Wu, Q., Yu, S., Hao, N., Wells, T., Meng, X., Li, M., Pu, Y., Liu, S., Ragauskas, A.J., 2017. Characterization of products from hydrothermal carbonization of pine. Bioresour. Technol. 244, 78–83. https://doi.org/10.1016/j.biortech.2017.07.138.
Yan, W., Perez, S., Sheng, K., 2017. Upgrading fuel quality of moso bamboo via low temperature thermochemical treatments: dry torrefaction and hydrothermal carbonization. Fuel 196, 473–480. https://doi.org/10.1016/j.fuel.2017.02.015.
Yao, Z., Ma, X., 2018. Characteristics of co-hydrothermal carbonization on polyvinyl chloride wastes with bamboo. Bioresour. Technol. 247, 302–309. https://doi.org/10.1016/j.biortech.2017.09.098.
You, S., Tong, H., Armin-Hoiland, J., Tong, Y.W., Wang, C.H., 2017. Techno-economic and greenhouse gas savings assessment of decentralized biomass gasification for electrifying the rural areas of Indonesia. Appl. Energy 208, 495–510. https://doi.org/10.1016/j.apenergy.2017.10.001.
Yuan, H., Wang, Y., Kobayashi, N., Zhao, D., Xing, S., 2015. Study of fuel properties of torrefied municipal solid waste. Energy Fuels 29, 4976–4980. https://doi.org/10.1021/ef502277u.
Zaccariello, L., Mastellone, M.L., 2015. Fluidized-bed gasification of plastic waste, wood, and their blends with coal. Energies 8, 8052–8068. https://doi.org/10.3390/en8088052.
Zhang, C., Ma, X., Huang, T., Zhou, Y., Tian, Y., 2020. Co-hydrothermal carbonization of water hyacinth and polyvinyl chloride: optimization of process parameters and characterization of hydrochar. Bioresour. Technol. 314, 123676. https://doi.org/10.1016/j.biortech.2020.123676.
Zhao, K., Li, Y., Zhou, Y., Guo, W., Jiang, H., Xu, Q., 2018. Characterization of hydrothermal carbonization products (hydrochars and spent liquor) and their biomethane production performance. Bioresour. Technol. 267, 9–16. https://doi.org/10.1016/j.biortech.2018.07.006.